A Comparison of Lattice-Matched GaInNAs and Metamorphic InGaAs Photodetector Devices

David B. Jackrel, Homan B. Yuen, Seth R. Bank, Mark A. Wistey, Xiaojun Yu, Junxian Fu, Zhilong Rao, and James S. Harris, Jr.
Stanford University, Solid State Research Lab, 420 Via Palou,
Stanford, CA 94305-4070, U.S.A.

ABSTRACT

The dilute-nitride GaInNAs shows great promise in becoming the next choice for 1 eV photodetector and multi-junction photovoltaic applications due to the ability for it to be grown lattice-matched on GaAs substrates. This paper will present results from high-power photodetector devices fabricated from high-quality thick GaInNAs and metamorphic InGaAs materials grown by MBE. The internal quantum efficiency of rear-illuminated PIN photodiodes with thick GaInNAs films as the intrinsic region (roughly 62% at 1064 nm) is somewhat lower than comparable metamorphic InGaAs devices (roughly 75% at 1064 nm). However, the dark current density of the GaInNAs devices is also somewhat lower (roughly 3 $\mu A/cm^2$ at $2x10^4$ V/cm bias) than the InGaAs devices (roughly 20 $\mu A/cm^2$ at $2x10^4$ V/cm bias), while the breakdown voltages (beyond -20 V) are comparable. Materials characterization of each structure, including x-ray diffraction and room-temperature as well as temperature-dependent photoluminescence studies will be presented in order to explain the characteristics observed in the devices composed of the two different material systems.

INTRODUCTION

The dilute-nitride GaInNAs shows great promise in becoming the next choice for 1 eV photodetector and multi-junction photovoltaic applications due to the ability for it to be grown lattice-matched on GaAs substrates. GaAs-based photodetector devices have several advantages over InP-based devices, such as substrate cost, convenience of processing, and heterojunction energy band engineering parameters. The current world record photovoltaic cell, produced by Spectrolab, is a triple junction structure composed of GaInP/GaAs/Ge with a power conversion efficiency of over 37% [1]. In order to further maximize the power conversion of the solar spectrum 4- and 5-junction cells with a 1.0 eV sub-cell lattice-matched to GaAs and Ge , such as a sub-cell composed of GaInNAs, must be developed [2]. Metamorphic InGaAs is the current choice for 1 eV materials grown on GaAs substrates. Historically, however, higher threading dislocation densities and rough interfaces plague these devices due to the large concentration of misfit dislocations inherent to metamorphic structures [3].

In order to create photodetectors capable of absorbing large amounts of laser power, and photovoltaic devices capable of withstanding high solar concentration ratios, rear-illuminated device architectures were developed. The absorbing layers of the rear-illuminated devices are directly adjacent to the heat sink thereby enhancing the thermal conductivity by orders of magnitude over conventional front-illuminated detectors. This results in devices with excellent linearity and very high damage thresholds. The most detrimental characteristic of rear-illuminated devices is that large fractions of the incident radiation are absorbed in the thick

moderately heavily doped substrate. In order to overcome this parasitic absorption, methods must be developed to thin the device substrate after bonding to a suitable heat sink.

EXPERIMENT

Lattice-matched GaInNAs and metamorphic InGaAs double-heterostructure PIN diodes (Figure 1 and Figure 2) were grown on (100) GaAs substrates using a load-locked Varian Mod. Gen II solid-source molecular beam epitaxy (MBE) machine with nitrogen supplied by an SVT Associates Model 4.5 RF-plasma cell. The intrinsic GaInNAs material is 1 μm thick, composed of approximately 1% N and approximately 8% In, and has a p-type doping of roughly 10^{16} cm^{-3}. The intrinsic InGaAs material is 2 microns thick, composed of approximately 25% In, and has an n-type doping of roughly 10^{16} cm^{-3}. The N- and P- barrier layers of the GaInNAs devices are composed of GaAs, while the N- and P- layers of the InGaAs devices are composed of InAlAs with 25% In. The graded buffer layer of the InGaAs structures is composed of InAlAs in order to remain optically transparent to 1064 nm radiation with the indium content linearly increasing from zero up to 25%. After growth, annealing was performed on the nitride materials using a rapid thermal anneal with arsenic out-diffusion limited by a GaAs proximity cap.

Rear-illuminated photodetector and photovoltaic mesa devices with 3 mm diameter active areas were processed at the Stanford Nanofabrication Facility. The heat sink for the devices was a high thermal conductivity aluminum nitride ceramic. Several front-illuminated GaInNAs photovoltaic devices were also processed and characterized at the National Renewable Energy Laboratory (NREL).

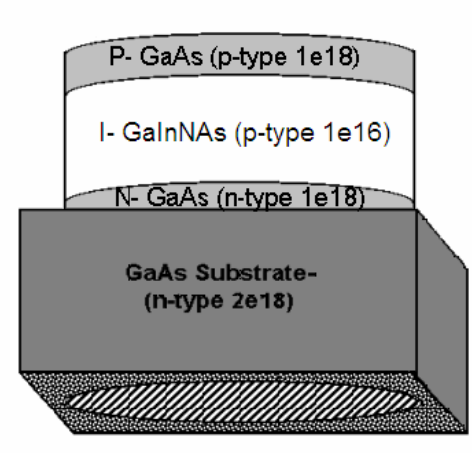

Figure 1. Lattice-matched GaInNAs structure.

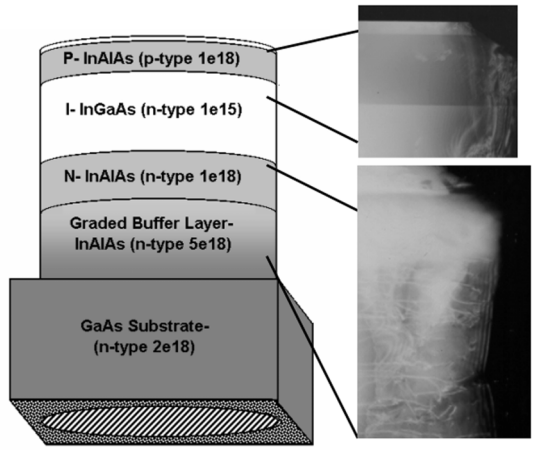

Figure 2. Metamorphic InGaAs structure and TEM images.

X-ray diffraction measurements were performed using a Phillips X'Pert PRO diffractometer. Room-temperature and temperature-dependent photoluminescence (PL) measurements were performed using a using a multi-line Ar+ laser as the excitation source, with luminescence collected and focused into a grating spectrometer and detected by an uncooled InGaAs photodiode and lock-in amplifier. All PL spectra were corrected for the wavelength response of the measurement system. Photocurrent and quantum efficiency measurements were performed

with a 1064 nm Nd:YAG NPRO laser from Lightwave and a Hewlett-Packard 4186A semiconductor parameter analyzer, and photovoltaic measurements were performed using an AM 1.5 solar simulator.

RESULTS AND DISCUSSION

Materials Characterization

TEM images of the metamorphic structure in Figure 2 show the dislocations confined to the graded buffer layer with no dislocations observed in the active layers. X-ray diffraction reciprocal space mapping allows one to directly measure both the in-plane and out-of-plane lattice constants of a crystal by utilizing a triple-axis measurement [4]. The reciprocal space maps of the structures confirm that the lattice-matched material is coherent to the GaAs substrate and that the metamorphic material is nearly fully relaxed. Figure 3A shows the relaxed InGaAs and InAlAs layers in the metamorphic structure along the omega/2-theta direction. Figure 3B shows the GaInNAs peak remaining completely coherent to the GaAs substrate although slightly strained. The graded buffer layer creates the diffuse reflection between the substrate and film layers in the reciprocal space map of the metamorphic structure.

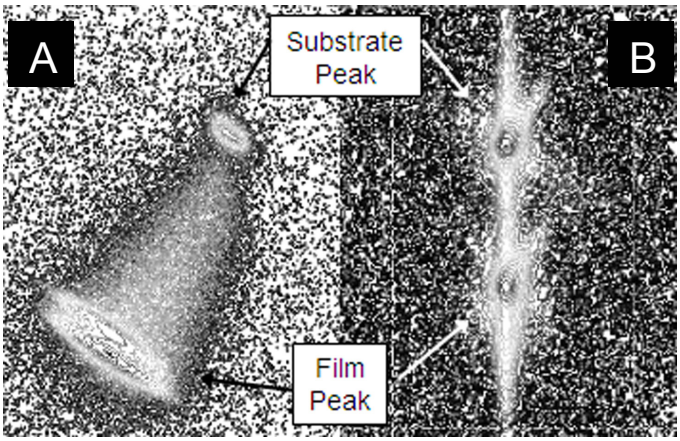

Figure 3. A. Metamorphic InGaAs, and B. lattice-matched GaInNAs XRD reciprocal space maps, both using (224) reflection.

Room-temperature PL measurements were performed to investigate the bandgap as well as optimize the post-growth annealing temperature by observing the relative intensity of radiative recombination in the GaInNAs materials (Figure 4). After growth, the GaInNAs structures were annealed at various temperatures, each for a duration of one minute, to reduce the number of non-radiative defects present in the as-grown (AG) material which quench the PL. The optimal annealing temperature was found to be 860°C, above which the PL intensity began to drop due to thermal damage. The as-grown material had a bandgap of roughly 1.01 eV which shifted to 1.08 eV after annealing.

Figure 5 compares the temperature dependence of the PL peak energy of the GaInNAs structures before and after annealing. The localization energy can be defined as the deviation from the Varshni equation at low temperatures [5] and is found to be reduced from 8.0 meV

before anneal to roughly 5.9 meV after annealing at 860°C. The localization of carriers has been attributed to fluctuations in the bandgap of the material caused by compositional inhomogeneities. InGaAs quantum well material has been found to have very little carrier localization (3-4 meV) [5]. Figure 6 shows the energy shift of the GaInNAs PL peaks from their respective energies at 20 K. The as-grown material has a discernable 3 meV rise in energy as the temperature is increased while the annealed material shows no such increase. This indicates that delocalized emission dominates in the annealed material, even at 20 K. The lower localization energy and the lack of a positive energy shift with increasing temperature both indicate that the compositional inhomogeneity as well as the concentration of non-radiative point defects is reduced with annealing. An increase in the magnitude of the carrier localization energy is correlated with reduced carrier diffusion lengths and decreased carrier lifetime. This is consistent with time-resolved PL that has shown that the carrier lifetime of the GaInNAs material in this study also increases with anneal (from 0.42 ns in the as-grown material to 0.55 ns after annealing at 860°C) [6].

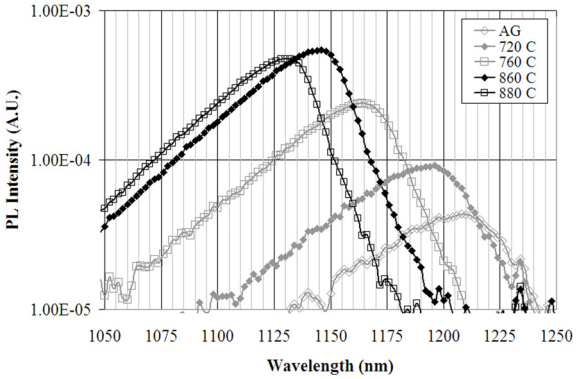

Figure 4. GaInNAs photoluminescence spectra at various post-growth annealing temperatures.

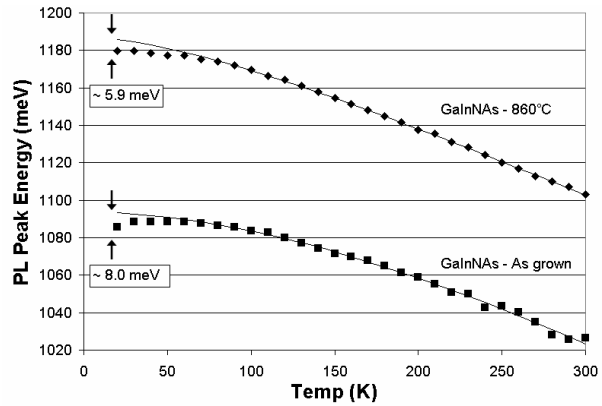

Figure 5. GaInNAs as-grown and optimally annealed temperature dependence of PL peak energy, solid lines represent Varshni fits.

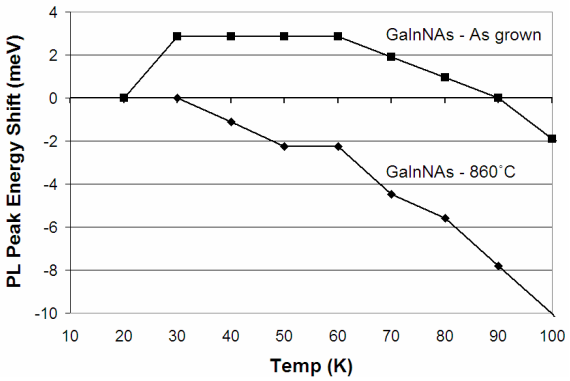

Figure 6. GaInNAs as-grown and optimally annealed temperature dependence of PL peak energy shift from 20-100 K.

Device Characterization

The photodetector internal quantum efficiency of various structures is plotted in Figure 7. The GaInNAs material annealed at the optimal temperature (860°C) shows much higher

efficiency than the GaInNAs material annealed at a temperature below the optimal value (720°C). The more ideal behavior of the optimally annealed material is consistent with the reduced localization energy at low-temperatures. The metamorphic InGaAs material, which has the lowest carrier localization energy, shows the highest device efficiency. The thinning of the substrate from roughly 500 μm to below 150 μm further improves the internal quantum efficiency of the rear-illuminated GaInNAs devices to roughly 62% at -4 V bias and the InGaAs devices to roughly 75%. Approximately 13% of the light is absorbed in the 150 μm substrate, thus the internal quantum efficiency of the InGaAs devices, accounting the parasitic absorption by the substrate, is nearly 90%, and similarly roughly 75% for the GaInNAs devices. Both sets of devices have displayed breakdown voltages beyond -20 V, and passively cooled rear-illuminated devices have absorbed intensities greater than 2.5 kW/cm^2 (20 W of 1064 nm light, with 1 mm spot size) under open-circuit conditions without showing any signs of damage.

The photovoltaic current-voltage responses under illumination by an AM 1.5 solar simulator spectrum for various devices are shown in Figure 8. The rear-illuminated (R-I) InGaAs devices show the highest short-circuit current due to their high quantum efficiency. However, the InGaAs devices show the lowest open-circuit voltage. The front-illuminated (F-I) GaInNAs device shows higher short-circuit current than the rear-illuminated device due to elimination of substrate absorption. The fill factors of the GaInNAs devices are slightly lower than the InGaAs devices due to the larger number of point defects in these materials, leading to recombination and non-ideal diode character.

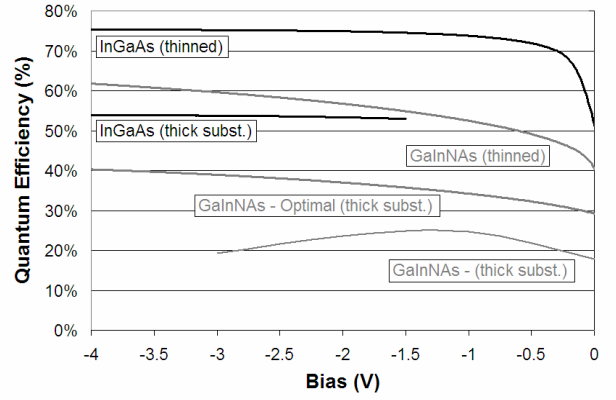

Figure 7. InGaAs and GaInNAs photodetector Internal quantum efficiency

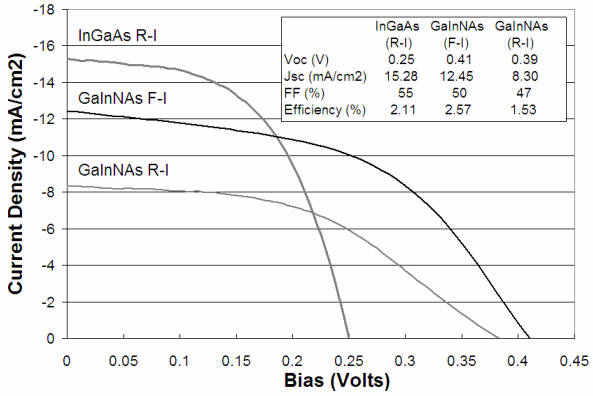

Figure 8. R-I and F-I InGaAs and GaInNAs photovoltaic device data.

Figure 9 shows the dark current and photocurrent densities of the thinned rear-illuminated InGaAs and GaInNAs devices. The InGaAs devices have much greater leakage current (roughly 20 μA/cm^2 at 2x10^4 V/cm bias) than the GaInNAs devices (roughly 3 μA/cm^2 at 2x10^4 V/cm bias) which can explain the low open-circuit voltage of the photovoltaic devices. However, the breakdown voltage of both the InGaAs and GaInNAs devices was found to be greater than -20 V. The increased leakage current in the InGaAs devices is most likely caused by a higher concentration of threading dislocations originating in the graded buffer layer, providing parallel current paths through the active region of the device. Figure 9 also illustrates that the signal-to-noise ratio of the GaInNAs devices (~10^5) is higher than that of the InGaAs devices (~10^4) due to the substantially lower dark current coupled with only slightly reduced device efficiency.

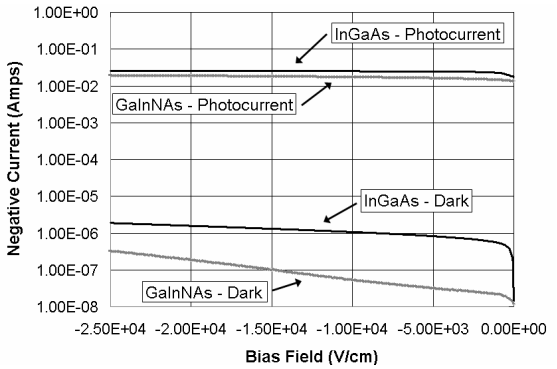

Figure 9. InGaAs and GaInNAs device dark current and photocurrent.

CONCLUSIONS

The as-grown thick GaInNAs materials have a substantial number of point defects and significant carrier localization. Post-growth rapid thermal anneal is required to reduce the number of point defects associated with non-radiative recombination and possibly to reduce compositional inhomogeneity that causes carrier localization. The optimal temperature for the rapid thermal anneal is 860°C. The effect of these improvements is longer carrier lifetimes which lead to higher photodetector internal quantum efficiencies. The InGaAs photodetector and photovoltaic devices have a higher internal quantum efficiency, but also larger leakage currents and lower open-circuit voltage. This indicates that although the point defect concentration of the InGaAs material is lower than that of the optimally annealed GaInNAs material, the threading dislocation density is most likely higher. Photodetector devices composed of GaInNAs also have significantly higher signal-to-noise ratio than similar InGaAs devices due to the reduced leakage current.

ACKNOWLEDGEMENTS

This material is based on work supported by the NSF under grants 9900793 and 0140297. The authors would like to thank Aaron Ptak at NREL in Golden, CO for the processing and characterization of the front-illuminated photovoltaic devices.

REFERENCES

1. R.R King *et al.*, 19th European Photovolt. Solar Energy Conf., Paris, France, 2004.
2. D.J. Friedman, J.F. Geisz and A.J. Ptak, in *Optoelectronic Properties of Semiconductors and Superlattices, Vol. 21: Physics and Applications of Dilute Nitrides*, edited by I.A. Buyanova and W.M. Chen (Taylor and Francis, New York, 2004), pp. 371-393.
3. Romanato et al., J. Appl. Phys. **86**, 4748-4755 (1999).
4. J.W. Eldredge, *et al.*, J. Vac. Sci. Technol. B **13**(2), 689-691, (1995).
5. M.A. Pinault and E. Tournie, Appl. Phys. Lett. **78**, 1391 (2001).
6. D. Jackrel, Homan Yuen, Junxian Fu, Seth Bank, Xiaojun Yu, Zhilong Rao, and James S. Harris, 31st IEEE Photovolt. Specialists Conf. Proceedings, 2005.